



Review

Phase relations of NASICON materials and compilation of the quaternary phase diagram $\text{Na}_2\text{O}-\text{P}_2\text{O}_5-\text{SiO}_2-\text{ZrO}_2$

Frank Tietz^{1,2,*}

¹ Forschungszentrum Jülich GmbH, Institute of Energy and Climate Research (IEK-1), Materials Synthesis and Processing (IEK-1), 52425 Jülich, Germany

² Helmholtz-Institute Münster, Forschungszentrum Jülich GmbH, 52425 Jülich, Germany

* **Correspondence:** Email: f.tietz@fz-juelich.de; Tel: +49-2461-615007; Fax: +49-2461-612455.

Abstract: A short overview is given on existing phase relations in the four related ternary diagrams, setting the frame for a quaternary phase diagram. On the basis of published data the three-dimensional phase region of NASICON materials is constructed and phase relations to ternary and binary systems as well as to single oxides are presented. To date, the NASICON region can be described as a compressed tetrahedron within the tetrahedral phase diagram. However, the three-dimensional presentation clearly elucidates that few reported compositions exist outside this compressed tetrahedron indicating that the phase region of NASICON materials may be larger than the solid solutions known so far. The three-dimensional representation also better elucidates the regions connecting the edges of the NASICON tetrahedron with ternary and binary compounds as well as single oxides, i.e., ZrO_2 and ZrSiO_4 , Na_3PO_4 , sodium silicates and sodium zirconium silicates and gives a better understanding of phase formations during the processing of the ceramics. The implications of the formation of secondary phases and glass-ceramic composites are discussed in terms of technological applications.

Keywords: NASICON; phase diagram; sodium ion conductor; solid electrolyte; sodium phosphates; sodium silicates; thermodynamics

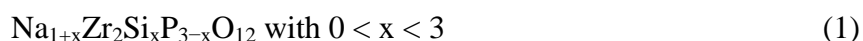
1. Introduction

The increasing need to harvest energy from fluctuating energy sources has placed energy storage into a central position for future energy technology scenarios. In the case of large-scale

stationary energy storage, sodium batteries seem to have advantages in comparison to lithium batteries in terms of production costs [1] due to the abundant availability of sodium and in terms of long-standing experience with large battery systems [2,3]. To date, in all sodium battery systems Na^+ - β'' -alumina has been employed for the solid electrolyte membrane. This is insofar surprising, as the processing of β'' -alumina to ceramic tubes is more elaborate, sophisticated and energy-consuming due to the high sintering temperatures [4] than for the only existing alternative: ceramics in the $\text{Na}_2\text{O-P}_2\text{O}_5\text{-SiO}_2\text{-ZrO}_2$ system. Although these materials have been known since 40 years [5,6], to our knowledge there has never been a technological approach to replace β'' -alumina in sodium batteries apart from a very recent comparison of a ZEBRA battery cells [7]. Since $\text{Na}_2\text{O-P}_2\text{O}_5\text{-SiO}_2\text{-ZrO}_2$ ceramics can be processed at lower temperatures and have higher ionic conductivity [8] leading to lower internal cell resistance and the possibility of reducing the operating temperature of ZEBRA batteries [7], they are serious candidates for an engineering development integrating them into large batteries. However, reviewing the available literature on these materials in the recent decades reveals that the chemistry of the $\text{Na}_2\text{O-P}_2\text{O}_5\text{-SiO}_2\text{-ZrO}_2$ system appears to be rather complex, fragmented and sometimes even contradictory. In the present work, we do not only summarize existing knowledge, but also try to harmonize the individual results.

2. Ternary and Quaternary Compounds

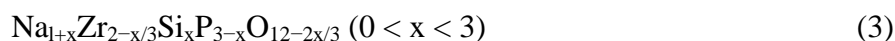
The Na^+ super-ionic conductor (NASICON) $\text{Na}_3\text{Zr}_2\text{Si}_2\text{PO}_{12}$ belongs to the solid solution [5].



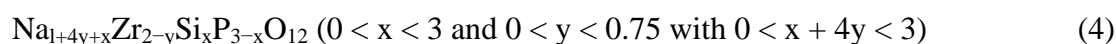
Its starting member, $\text{NaZr}_2\text{P}_3\text{O}_{12}$, also belongs to a series of ternary compositions which can be expressed in a general form as



crystallizing in the rhombohedral NASICON-type structure [5,9]. Compositions with distinct numbers of x are listed in Table 1. Since ZrO_2 was frequently observed as a second phase in sintered polycrystalline samples [10], Boilot et al. [11] reduced the ZrO_2 formation by reducing the zirconium content in the starting composition and found NASICON compositions with zirconium deficiency. Later von Alpen et al. [10] and Kohler et al. [12] confirmed the zirconium deficiency and proposed the substitution mechanisms



and



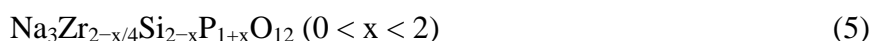
respectively, leading to a scientific dispute on the existence of NASICON materials with oxygen and/or zirconium vacancies [13,14]. Further crystallographic investigations on single crystals grown from sodium phosphate fluxes revealed a partial replacement of Zr^{4+} by four Na^+ ions up to $y = 1$ with $x = 0$ [15,16] (see Table 1) and $y = 1$ with $x = 0.5$ [17]. Therefore $\text{Na}_5\text{ZrP}_3\text{O}_{12}$ can be regarded as an end member for the pure phosphate, $\text{Na}_5\text{Zr}_{1.75}\text{Si}_3\text{O}_{12}$ for the pure silicate and $\text{Na}_{5.5}\text{ZrSi}_{0.5}\text{P}_{2.5}\text{O}_{12}$ [17], $\text{Na}_5\text{Zr}_{1.25}\text{SiP}_2\text{O}_{12}$ as well as $\text{Na}_5\text{Zr}_{1.5}\text{Si}_2\text{PO}_{12}$ for phosphate-silicates. However, crystal growth in the solidus region did not reveal the $\text{Zr} \leftrightarrow \text{Na}$ replacement mechanism [18]. Another observed

phenomenon in polycrystalline NASICON materials is the occurrence of glassy phases leading to the frequently used term “glass-ceramic” for these materials [19]. This phenomenon will be discussed below in more detail.

Table 1. The series $\text{Na}_{1+4x}\text{Zr}_{2-x}\text{P}_3\text{O}_{12}$ [5,17].

x	Abbreviation	Formula	Normalized to 3 (PO ₄) per formula unit	Considering also Zr ⁴⁺ ↔ Na ⁺ replacements
0	123	$\text{NaZr}_2\text{P}_3\text{O}_{12}$		
0.285	547	$\text{Na}_5\text{Zr}_4\text{P}_7\text{O}_{28}$	$\text{Na}_{2.14}\text{Zr}_{1.72}\text{P}_3\text{O}_{12}$	$\text{Na}_{1.86}(\text{Na}_{0.28}\text{Zr}_{1.72})\text{P}_3\text{O}_{12}$
0.33	759	$\text{Na}_7\text{Zr}_5\text{P}_9\text{O}_{36}$	$\text{Na}_{2.33}\text{Zr}_{1.67}\text{P}_3\text{O}_{12}$	$\text{Na}_2(\text{Na}_{0.33}\text{Zr}_{1.67})\text{P}_3\text{O}_{12}$
0.5	212	$\text{Na}_2\text{ZrP}_2\text{O}_8$	$\text{Na}_3\text{Zr}_{1.5}\text{P}_3\text{O}_{12}$	$\text{Na}_2(\text{Na}_{0.5}\text{Zr}_{1.5})\text{P}_3\text{O}_{12}$
0.8	725	$\text{Na}_7\text{Zr}_2\text{P}_5\text{O}_{17}$	$\text{Na}_{4.2}\text{Zr}_{1.2}\text{P}_3\text{O}_{12}$	$\text{Na}_{3.4}(\text{Na}_{0.8}\text{Zr}_{1.2})\text{P}_3\text{O}_{12}$
1	513	$\text{Na}_5\text{ZrP}_3\text{O}_{12}$		$\text{Na}_4(\text{NaZr})\text{P}_3\text{O}_{12}$

Besides the solid solution (1), charge compensation of Si ↔ P substitutions can also occur with Zr⁴⁺ vacancies instead of Na⁺ interstitial ions:



This series crystallizes in the monoclinic ($x < 0.5$) and rhombohedral ($x > 0.5$) NASICON-type structure [20], but also contains glassy amounts [21]. In addition, very recently during the synthesis of $\text{Na}_3\text{Zr}_2\text{Si}_2\text{PO}_{12}$ we observed phase stability and high conductivity despite a significant silicon deficiency [22]. This leads to a more fundamental consideration as to how substitutions or cation deficiencies in the polyanionic lattice may be compensated. In general, missing positive charges can be compensated by a) oxygen vacancies, b) partial zirconium addition and oxygen vacancies, c) partial sodium addition and oxygen vacancies, d) sodium addition and e) zirconium addition according to the series



respectively. These chemical observations and considerations are worth discussing in a wider frame (see Section 4).

Only very few reports exist on phase relations of series (1) establishing a quasi-ternary system [23] and giving relations of the end members in the ternary phase diagrams [24,25] which will be summarized in the next subsequent sections. So far, figures of quaternary phase diagrams have only been used to visualize the corresponding system under investigation without considering detailed phase relations [10,12,26]. Since the various possibilities of substitutions in NASICON materials, to our knowledge, have never been comprehensively discussed in relation to their neighboring phases, we present a first approach here of a quaternary phase diagram on the basis of existing thermodynamic studies and investigated compositions to date. We are aware that not all

available data correspond to each other when they are combined to a unified phase diagram, especially when isothermal phase diagrams were investigated at different temperatures. Nevertheless, focusing on the existing phases appearing in this quaternary system can still provide valuable information for further investigations on this complex family of solid electrolytes known as NASICON.

3. Ternary Phase Diagrams

In the following, the four ternary phase diagrams will be reviewed. For the sake of brevity, literature on binary systems is not mentioned, because it is cited in the publications of the ternary phase diagrams.

3.1. The Ternary System $\text{SiO}_2\text{-ZrO}_2\text{-P}_2\text{O}_5$

The detailed investigation of the system $\text{SiO}_2\text{-ZrO}_2\text{-P}_2\text{O}_5$ [27] revealed the compositions SiP_2O_7 (in low- and high-temperature form), $\text{Si}_2\text{P}_2\text{O}_9$, SiO_2 (α -cristobalite), $(\text{ZrO})_2\text{P}_2\text{O}_7$ (in metastable and stable form), ZrP_2O_7 (in low-temperature form) and ZrSiO_4 . No ternary compounds were found, only an extended phase width for $(\text{ZrO})_2\text{P}_2\text{O}_7$ up to $(\text{ZrO})_3\text{P}_4\text{O}_{13}$. According to this study, the resulting ternary phase diagram is shown in Figure 1.

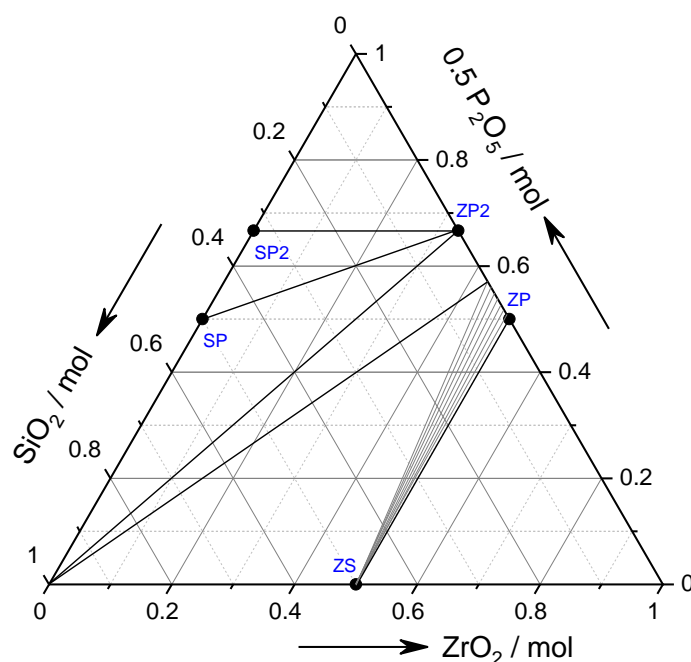


Figure 1. The ternary phase diagram $\text{SiO}_2\text{-ZrO}_2\text{-P}_2\text{O}_5$ according to Mason and Hummel [27]. The abbreviations denote the compositions $\text{Si}_2\text{P}_2\text{O}_9$ (SP), SiP_2O_7 (SP2), ZrP_2O_7 (ZP2), $(\text{ZrO})_2\text{P}_2\text{O}_7$ (ZP) and ZrSiO_4 (ZS). The gray lines starting at ZS correspond to a solid solution between ZP and ZP2. The subsolidus relations were determined at about 900 °C and between 1200 and 1625 °C for the regions $\text{SiO}_2\text{-ZP2-SP2}$ and $\text{SiO}_2\text{-ZrO}_2\text{-ZP2}$, respectively, indicating decreasing melting temperatures towards the upper left part of this phase diagram.

3.2. The Ternary System $\text{Na}_2\text{O}-\text{SiO}_2-\text{P}_2\text{O}_5$

A very comprehensive study of the $\text{Na}_2\text{O}-\text{SiO}_2-\text{P}_2\text{O}_5$ system was carried out by Turkdogan and Maddocks [28]. In total, ten binary sodium-containing oxides and three ternary compounds in the sodium-rich region were found. Among these, the stable composition $\text{Na}_{18}\text{P}_4\text{Si}_6\text{O}_{31}$ is of central importance, because it is linked with the other ternary compositions, a few binary compounds as well as several peritectic and eutectic points. Typically, the peritectics have melting points between 900 and 1000 °C, whereas the eutectic melting points vary from 1020 °C (close to N3S; for abbreviations, see caption of Figure 2) down to 780 °C (close to N2S3) on the silicate side. One eutectic on the phosphate side has an even lower melting point (550 °C between NP and N5P3).

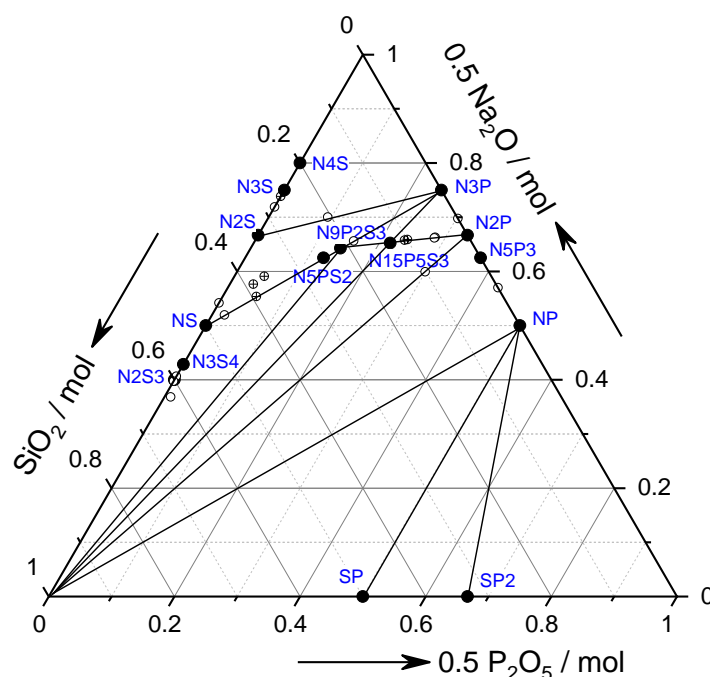


Figure 2. The ternary phase diagram $\text{SiO}_2-\text{P}_2\text{O}_5-\text{Na}_2\text{O}$ according to Turkdogan and Maddocks [28]. The two compositions SP and SP2 were added from Ref. [27]. The abbreviations along the binary axes denote the compositions $\text{Na}_2\text{Si}_3\text{O}_7$ (N2S3), $\text{Na}_6\text{Si}_8\text{O}_{19}$ (N3S4), $\text{Na}_2\text{Si}_2\text{O}_5$ (NS), Na_2SiO_3 (N2S), $\text{Na}_6\text{Si}_2\text{O}_7$ (N3S), Na_4SiO_4 (N4S), Na_3PO_4 (N3P), $\text{Na}_4\text{P}_2\text{O}_7$ (N2P), $\text{Na}_5\text{P}_3\text{O}_{10}$ (N5P3) and NaPO_3 (NP). The ternary compounds $\text{Na}_{10}\text{P}_2\text{Si}_4\text{O}_{18}$, $\text{Na}_{18}\text{P}_4\text{Si}_6\text{O}_{31}$ and $\text{Na}_{15}\text{P}_5\text{Si}_3\text{O}_{26}$ are abbreviated as N5PS2, N9P2S3, and N15P5S3, respectively. Along the lines of the subsolidus relations, the peritectic and eutectic points [22] are shown as crossed circles and open circles, respectively.

3.3. The Ternary System $\text{Na}_2\text{O}-\text{P}_2\text{O}_5-\text{ZrO}_2$

After identification of the ternary phosphates in Table 1 [5], the first steps towards a ternary $\text{Na}_2\text{O}-\text{P}_2\text{O}_5-\text{ZrO}_2$ phase diagram were undertaken by Milne and West [29,30]. They also identified N5ZP3 and N2ZP2 (for abbreviations, see caption of Figure 3) as NASICON-type materials as well as a solid solution of $\text{Na}_{5-4x}\text{Zr}_{1+x}\text{P}_3\text{O}_{12}$ with $0.04 < x < 0.11$ at 1000 °C and a solubility of Zr^{4+} in

Na_3PO_4 , i.e., $\text{Na}_{3-4x}\text{Zr}_x\text{PO}_4$, with $0 < x < 0.57$ [29]. Warhus adopted these results to a ternary phase diagram [24] specifying the phase equilibria at 1000 °C. The main features of the phase diagram were confirmed by Vlna et al. [31]. They also found four sodium phosphates, one sodium zirconate and four zirconium phosphates, in contrast to Ref. [27] (see Figure 1) but in agreement with Ref. [24]. The materials with NASICON-type structure lie on the join N3P-Z3P4 and can be described as $\text{Na}_{9-4y}\text{Zr}_y(\text{PO}_4)_3$. The end member phases N3P and NZ2P3 then correspond to $y = 0$ and 2, respectively, while for N5ZP3 and Z3P4 $y = 1$ and $y = 2.25$, respectively. The stated compound $\text{Na}_7\text{Zr}_{0.5}(\text{PO}_4)_4$ [9,30] is part of the solid solution $\text{Na}_{3-4x}\text{Zr}_x\text{PO}_4$ [29] and therefore not explicitly shown in Figure 3.

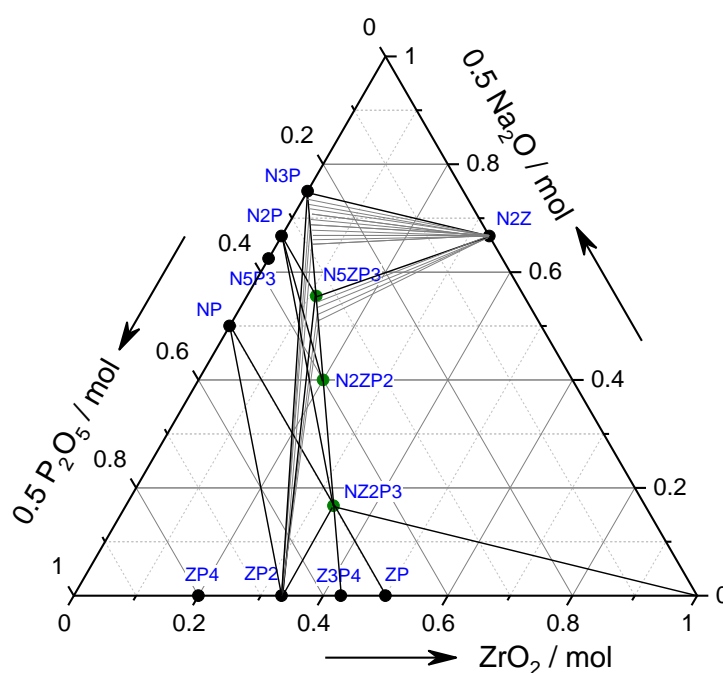


Figure 3. The ternary phase diagram $\text{P}_2\text{O}_5\text{-ZrO}_2\text{-Na}_2\text{O}$ according to Refs. [24,25,29,30,31]. The abbreviations denote the compositions Na_2ZrO_3 (N2Z), $\text{Zr}_2\text{P}_2\text{O}_9$ (ZP), $\text{Zr}_3\text{P}_4\text{O}_{16}$ (Z3P4), ZrP_2O_7 (ZP2) and $\text{ZrP}_4\text{O}_{12}$ (ZP4). The abbreviations of the sodium phosphates are given in the caption of Figure 1. The ternary compounds are already mentioned in Table 1 and marked with a green symbol to indicate the isostructural nature of the materials and to assign them as NASICON-type compositions. The gray lines starting at N2Z and ZP2 correspond to the existing solid solutions. The subsolidus relations were determined between 350 (for the phosphate-rich region) and 1000 °C.

3.4. The Ternary System $\text{Na}_2\text{O-SiO}_2\text{-ZrO}_2$

The first investigation of the system $\text{Na}_2\text{O-SiO}_2\text{-ZrO}_2$ revealed one sodium zirconate, four sodium silicates, all melting between 800 and 1100 °C, one zirconium silicate and three ternary compounds (N2ZS, N4Z2S3 and N2ZS2; for abbreviations see caption of Figure 4) [32]. In this study, seven eutectic points were also determined varying between 1000 and 1100 °C. On the basis

of these results, the subsolidus relations were determined [33,34] including N2S3. Later, Wilson and Glasser identified two more ternary compositions (N7ZS5, N2ZS4) and one additional sodium silicate (N3S4) with a very limited width of thermal stability [35]. Therefore, its phase relationships are presented as dash-dotted lines in Figure 4. Considering the phase equilibria at 1000 °C [24,25], the compounds N7ZS5 and N3S4 are not stable and a narrow region of melt exists (see gray area in Figure 4) indicating that the ternary compounds N2ZS4, N2ZS2 and N4Z2S3 are in equilibrium with the melt, ZS and ZrO_2 . Since eutectic points were observed in the sodium-rich region [32], the gray area can probably be extended to N4S, also affecting the phase relations of N2ZS.

The frequent observation of glassy phases and ZrO_2 as impurities in NASICON ceramics becomes understandable in Figure 4, because the compound N4Z2S3 is in equilibrium with these observed impurities. However, investigations of NASICON phase formation with different starting materials [36] have also shown the appearance of phosphate-rich segregations, predominantly Na_3PO_4 , indicating a partial de-mixing of the NASICON material to P- and Si-rich compositions. To avoid these reactions, processing of NASICON should be carried out below 1000 °C, but higher temperatures are required for obtaining dense ceramics so far.

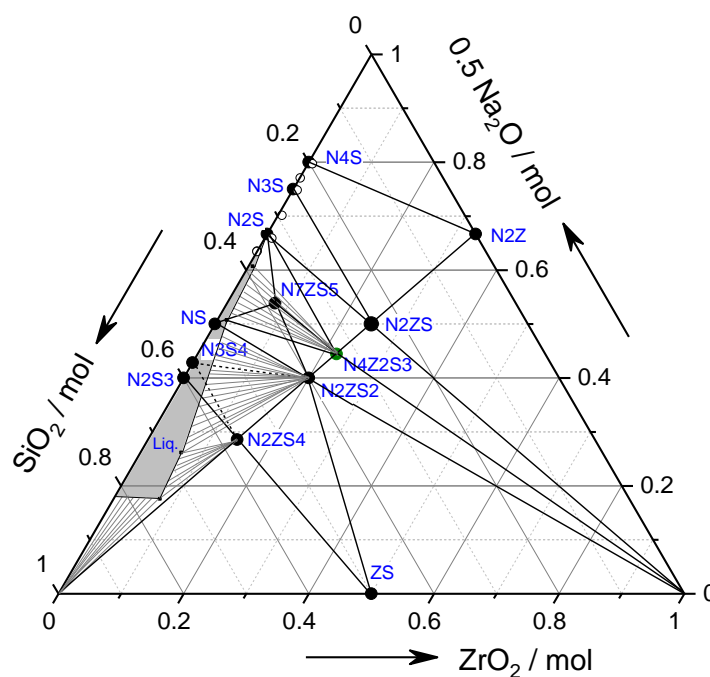


Figure 4. The ternary phase diagram $\text{SiO}_2\text{-ZrO}_2\text{-Na}_2\text{O}$ according to Refs. [24,25,32–35]. The abbreviations of the binary compounds are given in the previous figure captions. Those of the ternary compositions denote $\text{Na}_2\text{ZrSi}_4\text{O}_{11}$ (N2ZS4), $\text{Na}_2\text{ZrSi}_2\text{O}_7$ (N2ZS2), $\text{Na}_4\text{Zr}_2\text{Si}_3\text{O}_{12}$ (N4Z2S3), $\text{Na}_2\text{ZrSiO}_5$ (N2ZS), and $\text{Na}_{14}\text{Zr}_2\text{Si}_{10}\text{O}_{31}$ (N7ZS5). N4Z2S3 was marked with a green symbol to indicate of a NASICON material. The gray area tentatively represents a liquidus region at 1000 °C and the gray lines starting at N2ZS4, N2ZS2 and N4Z2S3 correspond to the solid solutions with sodium silicates and silica [24,25]. Small open circles indicate eutectic points along the sodium silicate region [32].

4. The Quaternary System $\text{Na}_2\text{O-SiO}_2\text{-P}_2\text{O}_5\text{-ZrO}_2$

Using the existing knowledge on the ternary systems as well as the reported stability region of materials crystallizing with NASICON structure, i.e., the solid solutions and individual compositions of single crystals investigated, a tentative three-dimensional phase field of NASICON materials was established in a quaternary phase diagram. It has the shape of a compressed tetrahedron (blue region in Figure 5). Three of the edges of the tetrahedron are defined by the solid solutions (1), (2) and (3), indicated as solid red lines in Figure 5. An additional side of the tetrahedron is defined by the two-dimensional solid solution (4), represented by the mesh of blue lines. In general, the blue tetrahedron displays the chemical formula



proposed by Rudolf et al. [37,38], which contains many possible non-stoichiometric variations (Si/P substitution, Zr/Na substitution, Zr and O deficiency). It should be kept in mind, however, that from the thermodynamic point of view the blue triangle is not strictly a single-phase region. It rather represents a region in which the NASICON phase appears with predominant volume fraction. In most of the compositions, especially those towards high SiO_2 content [3], the obtained samples also contain a homogeneous distribution of glassy phase [21,39,40]. However, in samples with the NASICON composition $\text{Na}_3\text{Zr}_2\text{Si}_2\text{PO}_{12}$ (large black circle in Figures 5 and 6; see arrow in Figure 5) glass formation increases with increasing sintering temperature and dwell time at high temperature [26,41], mainly induced by the evaporation of Na_2O from the sample surface leading to ZrO_2 precipitation and partial de-mixing of the NASICON phase [42]. Typically, the compositional separation is accompanied by accelerated grain growth due to liquid-phase sintering, which can be used to prepare single crystals with crystal edges of about 50–300 μm [12,42,43]. An example of the resulting microstructure revealing the different phenomena in a sintered body is shown in Figure 7.

It is worth noting, however, that the phase formation during sintering in air can lead to different results than during phase diagram studies using closed capsules for annealing samples [9,24,41]. The discrepancies mainly result from the different partial pressure of Na_2O to which the samples are exposed. The loss of Na_2O during sintering is frequently compensated by the addition of a sodium source during powder synthesis, but it usually remains unclear as to whether the additional amounts really match the losses during heat treatment. An excess of 10 at.% of sodium can, however, substantially increase the ionic conductivity [44] and mainly influences the grain boundary conductivity at ambient temperatures.

Based on the knowledge of appearing additional phases, the green areas in Figure 5 show the regions connecting the edges of the NASICON tetrahedron with binary compounds and single oxides, i.e., ZrO_2 and ZrSiO_4 [23], Na_3PO_4 and the sodium silicates ranging from $\text{Na}_2\text{Si}_2\text{O}_5$ to $\text{Na}_6\text{Si}_2\text{O}_7$. Depending on the temperature, the phase equilibria may be more extended from SiO_2 to Na_4SiO_4 as indicated by a different transparency of the large triangle in Figure 5. For Zr-deficient and Si-rich NASICON compositions, phase relations were observed towards ternary compounds (N2ZS2 and N2ZS4) [23], in analogy to Figure 4 and are shown as yellow areas in Figure 5.

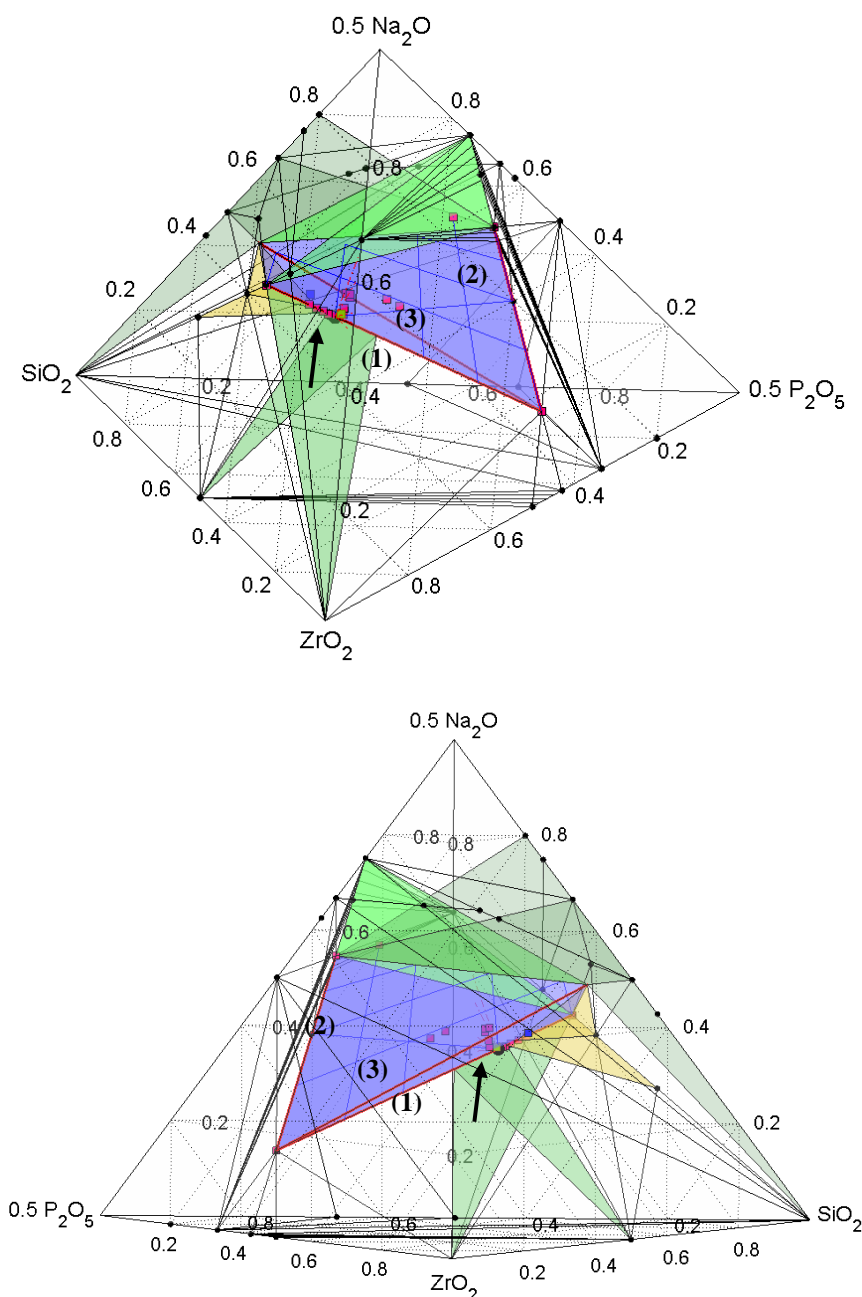


Figure 5. Two different views on the quaternary phase diagram $\text{Na}_2\text{O}-\text{SiO}_2-\text{ZrO}_2-\text{P}_2\text{O}_5$ displaying the phase field of NASICON materials as a blue compressed tetrahedron. The three edges of the tetrahedron marked as solid red lines are the solid solutions (1), (2) and (3). One side of the tetrahedron is defined by the two-dimensional solid solution (4) represented by the mesh of blue lines. The green areas show the regions connecting the edges of the NASICON tetrahedron with ZrO_2 , Na_3PO_4 and the sodium silicates ranging from SiO_2 to Na_4SiO_4 , whereas the yellow areas mark the phase relations to N2ZS2 and N2ZS4. For the sake of orientation, the NASICON composition $\text{Na}_3\text{Zr}_2\text{Si}_2\text{PO}_{12}$ is marked as a black circle (see arrow). Single crystals investigated by diffraction methods are indicated as red squares [12,14–19,37,38,42]. Unusual compositions of polycrystalline materials are shown as blue [10,39] and green [22] squares.

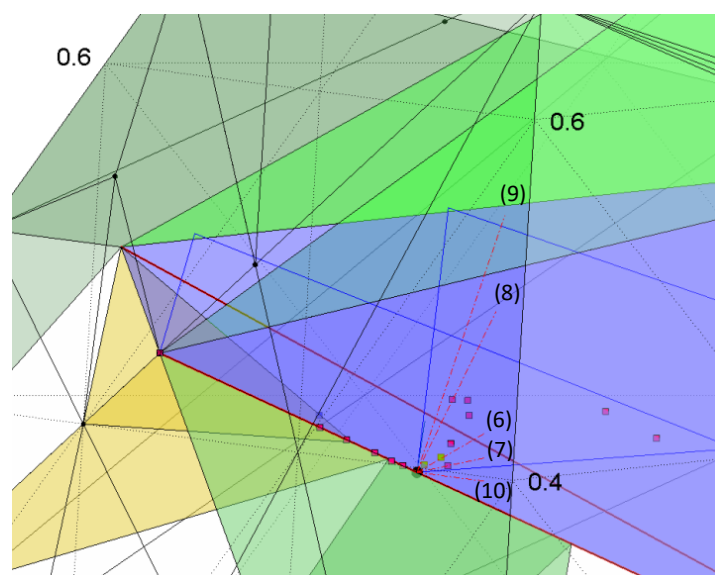


Figure 6. Enlarged view of the quaternary phase diagram $\text{Na}_2\text{O}-\text{SiO}_2-\text{ZrO}_2-\text{P}_2\text{O}_5$ around the NASICON composition $\text{Na}_3\text{Zr}_2\text{Si}_2\text{PO}_{12}$ (black circle). The dashed-dotted red lines represent the series (6) to (10). For the other symbols and colored surfaces, see caption of Figure 5.

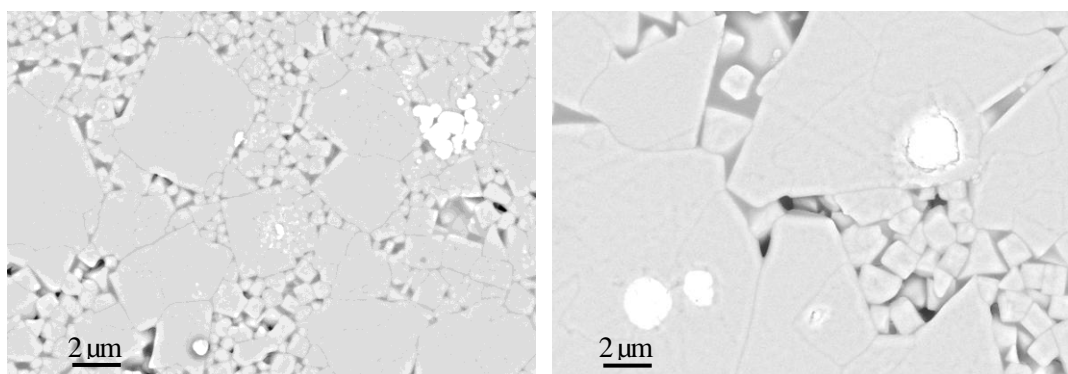


Figure 7. Microstructure of a $\text{Na}_3\text{Zr}_2\text{Si}_2\text{PO}_{12}$ ceramics sintered at $1250\text{ }^\circ\text{C}$ for 6 h (left) and 24 h (right). After polishing the cross sections, the samples were thermally etched for better identification of the grains and grain boundaries. From the backscattering electron images, the occurring phases can clearly be distinguished: ZrO_2 (white), NASICON (light gray), glass (middle gray) and pores (black). Note the significantly different grain sizes due to the varied dwell time at $1250\text{ }^\circ\text{C}$.

To date, only a few individual compositions, e.g., $\text{Na}_{3.1}\text{Zr}_{1.55}\text{Si}_{2.3}\text{P}_{0.7}\text{O}_{11}$ [10,39], $\text{Na}_{5.5}\text{ZrSi}_{0.5}\text{P}_{2.5}\text{O}_{12}$ [17], and $\text{Na}_{2.95}\text{Zr}_{1.92}\text{Si}_{1.81}\text{PO}_{11.44}$ [22] have been found outside the blue triangle. Normalizing the latter composition to twelve oxygen ions per formula unit, it can also be written as $\text{Na}_{3.09}\text{Zr}_{2.01}\text{Si}_{1.90}\text{P}_{1.05}\text{O}_{12}$, but the position in the phase diagram remains. Therefore, the stability region of NASICON materials seems to be larger than indicated in Figure 5 and more systematic work is necessary to determine the whole stability region of NASICON materials.

Individual compositions which were refined by single-crystal X-ray or neutron diffraction are

shown in Figures 5 and 6 as red squares [12,14–19,37,38,42]. The blue square denotes the unusual composition $\text{Na}_{3.1}\text{Zr}_{1.55}\text{Si}_{2.3}\text{P}_{0.7}\text{O}_{11}$ of von Alpen et al. [10] and the light-green squares correspond to the Si-deficient compositions reported by Naqash et al. [22]. The dashed red lines starting at the black circle ($\text{Na}_3\text{Zr}_2\text{Si}_2\text{PO}_{12}$) indicate the series (6) to (10) as a possible charge compensation mechanism for Si-deficient compositions as mentioned in the introductory part of this paper. The related green squares are located along series (6) (Figure 6). However, a more extended study is necessary to elucidate the phase stabilities and substitution rules in this region of the phase diagram.

5. Conclusions

With respect to technological application, several conclusions can be drawn from the existing knowledge and Figure 5:

- So far, the highest conductivity of NASICON materials within the discussed quaternary system can be attributed to the region of series (1) with $2 < x < 2.5$ [5,45], to compositions with similar Si/P ratio but with a Zr deficiency [10,39] or Si deficiency [22]. In other words, high ionic conductivity is not restricted to series (1) despite the fact that Si-rich compositions and especially those with Zr deficiency show a substantial fraction of glassy phase [39]. In turn, this implies that the glass either has a high conductivity or that the glass only exists at high temperatures and crystallizes with a NASICON structure during cooling. Preliminary μ -Raman measurements suggest the latter interpretation (Giarola M and Mariotto G, personal communication, University of Verona). However, since only a few reports are available on “offside” compositions from series (1), more systematic investigations in this region of the phase diagram are necessary to explore the full potential of NASICON materials.
- Taking glass formation as an unavoidable process during component manufacturing, the distribution of the Si-rich glass as an outer shell around the P-rich NASICON crystals (Figure 7) can be used as an intrinsic protection layer against reduction with metallic sodium in battery developments. If a continuous glass film is realized, the higher thermodynamic stability of the silicates can protect the NASICON phase from phosphide formation [25,39,46]. Although such glass-rich compositions show very high ionic conductivity [10,39], this additional phase contributes to the total resistance like an enlarged grain boundary resistance which should be minimized. In addition, the crystallized glassy phase may have significant influence on the mechanical properties [7], which need to be addressed and systematically investigated.
- This thermodynamic benefit of the glass phase also implies a practical drawback: Sintering of ceramics, especially for plates and larger components becomes more difficult. On the one hand, the ceramics tend to stick to the base plate and when thin components are considered, they can easily break during detachment from the base plate. On the other hand, large components like tubes may deform more easily during hanging sintering due to the low mechanical strength of the materials and viscous flow at high temperatures.

Acknowledgments

The author thanks Prof. Mike A. Scarpulla (University of Utah, Depts. of Electrical & Computer Engineering and Materials Science & Engineering) for helpful initial advice to use the MATLAB software and Dr. Robert Mücke (IEK-1) for important computational support. Sahir Naqash and Dr.

Doris Sebold (both IEK-1) are gratefully acknowledged for sample preparations and SEM images, respectively.

Conflict of Interest

The author declares no conflict of interest related to the content of this publication.

References

1. Larcher D, Tarascon JM (2015) Towards greener and more sustainable batteries for electrical energy storage. *Nat Chem* 7: 19–29.
2. Doughty DH, Butler PC, Akhil AA, et al. (2010) Batteries for Large-Scale Stationary Electrical Energy Storage. *Electrochem Soc Interface* 19: 49–53.
3. Benato R, Cosciani N, Crugnola G, et al. (2015) Sodium nickel chloride battery technology for large-scale stationary storage in the high voltage network. *J Power Sources* 293: 127–136.
4. Lu X, Xia G, Lemmon JP, et al. (2010) Advanced materials for sodium-beta alumina batteries: Status, challenges and perspectives. *J Power Sources* 195: 2431–2442.
5. Hong HYP (1976) Crystal Structure and Crystal Chemistry in the System $\text{Na}_{1+x}\text{Zr}_2\text{Si}_x\text{P}_{3-x}\text{O}_{12}$. *Mater Res Bull* 11: 173–182.
6. Goodenough JB, Hong HYP, Kafalas JA (1976) Fast Na^+ -Ion Transport in Skeleton Structures. *Mater Res Bull* 11: 203–220.
7. Kim J, Jo SH, Bhavaraju S, et al. (2015) Low temperature performance of sodium–nickel chloride batteries with NaSICON solid electrolyte. *J Electroanal Chem* 759: 201–206.
8. May GJ, Hooper A (1978) The effect of microstructure and phase composition on the ionic conductivity of magnesium-doped sodium-beta-alumina. *J Mater Sci* 13: 1480–1486.
9. Clearfield A, Guerra R, Oskarsson A, et al. (1983) Preparation of Sodium Zirconium Phosphates of the Type $\text{Na}_{1+4x}\text{Zr}_{2-x}(\text{PO}_4)_3$. *Mater Res Bull* 18: 1561–1567.
10. von Alpen U, Bell MF, Höfer HH (1981) Compositional Dependence of the Electrochemical and Structural Parameters in the NASICON System ($\text{Na}_{1+x}\text{Si}_x\text{Zr}_2\text{P}_{3-x}\text{O}_{12}$). *Solid State Ionics* 3–4: 215–218.
11. Boilot JP, Salani é JP, Desplanches G, et al. (1979) Phase Transformation in $\text{Na}_{1+x}\text{Si}_x\text{Zr}_2\text{P}_{3-x}\text{O}_{12}$ Compounds. *Mater Res Bull* 14: 1469–1477.
12. Kohler H, Schultz H, Melnikov O (1983) Composition and Conduction Mechanism of the NASICON Structure—X-Ray Diffraction Study on two Crystals at Different Temperatures. *Mater Res Bull* 18: 1143–1152.
13. Tsai CL, Hong HYP (1983) Investigation of phases and stability of solid electrolytes in the NASICON system. *Mater Res Bull* 18: 1399–1407.
14. Clearfield A, Subramanian MA, Wang W, et al. (1983) The Use of Hydrothermal Procedures to Synthesize NASICON and Some Comments on the Stoichiometry of NASICON Phases. *Solid State Ionics* 9–10: 895–902.
15. Kohler H, Schultz H (1985) NASICON Solid Electrolytes Part I: The Na^+ -Diffusion Path and Its Relation to the Structure. *Mater Res Bull* 20: 1461–1471.
16. Boilot JP, Collin G, Comes R (1983) Zirconium Deficiency in NASICON-Type Compounds: Crystal Structure of $\text{Na}_5\text{Zr}(\text{PO}_4)_3$. *J Solid State Chem* 50: 91–99.

17. Boilot JP, Collin G, Comes R (1983) Stoichiometry and phase transitions in NASICON type compounds. *Solid State Ionics* 9–10: 829–834.
18. Boilot JP, Collin G, Colomban Ph (1987) Crystal Structure of the True NASICON: $\text{Na}_3\text{Zr}_2\text{Si}_2\text{PO}_{12}$. *Mater Res Bull* 22: 669–676.
19. Boilot JP, Colomban Ph, Collin G (1988) Stoichiometry-Structure-Fast Ion Conduction in the NASICON Solid Solution. *Solid State Ionics* 28–30: 403–410.
20. Lucco-Borlera M, Mazza D, Montanaro L, et al. (1997) X-ray characterization of the new NASICON compositions $\text{Na}_3\text{Zr}_{2-x/4}\text{Si}_{2-x}\text{P}_{1+x}\text{O}_{12}$ with $x = 0.333, 0.667, 1.000, 1.333, 1.667$. *Powder Diffr* 12: 171–174.
21. Bohnke O, Ronchetti S, Mazza D (1999) Conductivity measurements on NASICON and nasicon-modified materials. *Solid State Ionics* 122: 127–136.
22. Naqash S, Ma Q, Tietz F, et al. (2017) $\text{Na}_3\text{Zr}_2(\text{SiO}_4)_2(\text{PO}_4)$ prepared by a solution-assisted solid state reaction. *Solid State Ionics* 302: 83–91.
23. Engell J, Mortensen S, Møller L (1983) Fabrication of NASICON Electrolytes from Metal Alkoxide Derived Gels. *Solid State Ionics* 9–10: 877–884.
24. Warhus U (1986) Synthese und Stabilität des NASICON Mischkristallsystems $(\text{Na}_{1+x}\text{Zr}_2\text{Si}_x\text{P}_{3-x}\text{O}_{12}, 0 \leq x \leq 3)$ [PhD thesis]. University of Stuttgart.
25. Kreuer KD, Kohler H, Maier J (1989) Sodium Ion Conductors with NASICON Framework Structure, In: Takahashi T, *High Conductivity Ionic Conductors: Recent Trends and Application*, Singapore: World Scientific Publishing Co., 242–279.
26. Warhus U, Maier J, Rabenau A (1988) Thermodynamics of NASICON $(\text{Na}_{1+x}\text{Zr}_2\text{Si}_x\text{P}_{3-x}\text{O}_{12})$. *J Solid State Chem* 72: 113–125.
27. Mason TO, Hummel FA (1974) Compatibility Relations in the System $\text{SiO}_2\text{-ZrO}_2\text{-P}_2\text{O}_5$. *J Am Ceram Soc* 57: 538–539.
28. Turkdogan ET, Maddocks WR (1952) Phase Equilibrium Investigation of the $\text{Na}_2\text{O-SiO}_2\text{-P}_2\text{O}_5$ Ternary System. *J Iron Steel Inst* 172: 1–15.
29. Milne SJ, West AR (1983) Compound formation and conductivity in the system $\text{Na}_2\text{O-ZrO}_2\text{-P}_2\text{O}_5$: Sodium zirconium orthophosphates. *Solid State Ionics* 9–10: 865–868.
30. Milne SJ, West AR (1985) Zr-Doped Na_3PO_4 : Crystal Chemistry, Phase Relations, and Polymorphism. *J Solid State Chem* 57: 166–177.
31. Vlana M, Petrosyan Y, Kovar V, et al. (1993) Phase Coexistence in the System $\text{Na}_2\text{O-P}_2\text{O}_5\text{-ZrO}_2$. *Chem Pap* 47: 296–297.
32. D'Ans J, Löffler J (1930) Untersuchungen im System $\text{Na}_2\text{O-SiO}_2\text{-ZrO}_2$. *Z Anorg Allg Chem* 191: 1–35.
33. Polezhaev YM, Chukhlantsev VG (1965) Triangulation of the System $\text{Na}_2\text{O-ZrO}_2\text{-SiO}_2$. *Izv Akad Nauk SSSR Neorg Mater* 1: 1990–1993; *Inorg Mater (Engl Transl)* 1: 1797–1800.
34. Sircar A, Brett NH (1970) Phase Equilibria in Ternary Systems Containing Zirconia and Silica, IV. Preliminary Study of the System $\text{Na}_2\text{O-ZrO}_2\text{-SiO}_2$. *Trans Brit Ceram Soc* 69: 131–135.
35. Wilson G, Glasser FP (1987) Subsolvus Phase Relations in the System $\text{Na}_2\text{O-ZrO}_2\text{-SiO}_2$. *Brit Ceram Trans J* 86: 199–201.
36. Nicholas VA, Heyns AM, Kingon AI, et al. (1986) Reactions in the formation of $\text{Na}_3\text{Zr}_2\text{Si}_2\text{PO}_{12}$. *J Mater Sci* 21: 1967–1973.
37. Rudolf PR, Subramanian MA, Clearfield A, et al. (1985) The Crystal Structure of a Nonstoichiometric NASICON. *Mater Res Bull* 20: 643–651.

38. Rudolf PR, Clearfield A, Jorgensen JD (1986) Rietveld Refinement Results on Three Nonstoichiometric Monoclinic NASICONs. *Solid State Ionics* 21: 213–224.
39. Yde-Andersen S, Lundgaard JS, Møller L, et al. (1984) Properties of NASICON Electrolytes Prepared from Alkoxide Derived Gels: Ionic Conductivity, Durability in Molten Sodium and Strength Test Data. *Solid State Ionics* 14: 73–79.
40. Perthuis H, Colomban Ph (1986) Sol-Gel Routes Leading to Nasicon Ceramics. *Ceram Int* 12: 39–52.
41. Maier J, Warhus U, Gmelin E (1986) Thermodynamic and Electrochemical Investigations of the NASICON Solid Solution System. *Solid State Ionics* 18–19: 969–973.
42. Boilot JP, Collin G, Colomban Ph (1988) Relation Structure-Fast Ion Conduction in the NASICON Solid Solution. *J Solid State Chem* 73: 160–171.
43. Colomban Ph (1986) Orientational Disorder, Glass/Crystal Transition and Superionic Conductivity in NASICON. *Solid State Ionics* 21: 97–115.
44. Park H, Jung K, Nezafati M, et al. (2016) Sodium Ion Diffusion in Nasicon ($\text{Na}_3\text{Zr}_2\text{Si}_2\text{PO}_{12}$) Solid Electrolytes: Effects of Excess Sodium. *ACS Appl Mater Interfaces* 8: 27814–27824.
45. Kafalas JA, Cava JR (1979) Effect of Pressure and Composition of Fast Na^+ -Ion Transport in the System $\text{Na}_{1+x}\text{Zr}_2\text{Si}_x\text{P}_{3-x}\text{O}_{12}$. Proceedings of the International Conference on Fast Ion Transport in Solids, 419–422.
46. Kreuer KD, Warhus U (1986) NASICON Solid Electrolytes: Part IV Chemical Durability. *Mater Res Bull* 21: 357–363.



AIMS Press

© 2017 Frank Tietz, licensee AIMS Press. This is an open access article distributed under the terms of the Creative Commons Attribution License (<http://creativecommons.org/licenses/by/4.0>)